Two-component lattice bosons with cavity-mediated long-range interaction

Xin Guan, Jingtao Fan, Xiaofan Zhou, Gang Chen,* and Suotang Jia
State Key Laboratory of Quantum Optics and Quantum Optics Devices, Institute of Laser Spectroscopy, Shanxi University, Taiyuan 030006, China
and Collaborative Innovation Center of Extreme Optics, Shanxi University, Taiyuan 030006, China

(Received 7 March 2019; published 15 July 2019)

In this paper, we consider a two-component atomic Bose lattice gas inside an optical cavity to explore a competition between the short-range collisional and cavity-mediated long-range interactions. Utilizing a self-consistent mean-field approach, we map out the ground-state phase diagrams showing the superfluid, lattice supersolid, Mott insulator, and spin-density wave phases. Unlike its single-component analog, this lattice supersolid is here characterized by the coexistence of the superfluid and the spin-density wave. Moreover, for the relatively small long-range interaction, the phase diagrams exhibit a correspondence between the parity of the lattice filling number and the spin imbalance. Finally, we propose how to detect the different quantum phases under current experimental setups.

DOI: 10.1103/PhysRevA.100.013617

I. INTRODUCTION

Recent experimental breakthrough of ultracold quantum gases in optical lattices has opened up a new avenue toward exploring quantum many-body physics [1–4]. The experimental feasibility to engineer lattice geometry using lasers and the tunability of interaction strength by Feshbach resonance make such system an excellent simulator of a vast kind of condensed matter phenomena [1]. However, the experiments are mostly limited to short-range collisional interactions [5–7], which hinders the further investigation of complex quantum phenomena originating from long-range interactions. Fortunately, the dynamical atom-photon coupling enhanced by an optical cavity offers a viable solution to overcome this drawback [8–12]. Through exchanging photons with a radiation field, ultracold atoms loaded inside a cavity-generated optical lattice can establish an indirect long-range interaction. Utilizing this setup, some judicious experiments have faithfully realized a long-range interaction between single component lattice bosons, and various quantum phases from competing short- and long-range interactions have been observed [9].

Apart from its motional character, internal degrees of freedom such as spin or quasispin in lattice models are at the heart of diverse novel physical phenomena [13–31]. This necessitates the introduction of additional internal components to lattice atomic gases, which may enrich the quantum simulating toolbox. As a matter of fact, a series of prominent cold atom experiments have realized multicomponent systems, such as Fermi-Bose [32,33], Fermi-Fermi [34], and Bose-Bose [35–37] mixtures. Theoretical interest in these systems is also tremendous. Notable examples include the prediction of exotic quantum phases which are exclusive to two-component lattice bosons, such as the supercounterfluid and pairsuperfluid phases [15,28,29]. The former corresponds to a zero net atomic superfluid current but nonzero currents of the component in opposite direction, while the latter refers to a superfluid of pairs where bosons of different components hop together in the lattice. Putting these fruitful achievements aside, novel perspectives on such systems may be gained by applying an additional dynamic cavity field, which imposes extra constraints on various degrees of freedom. Actually, it has been shown that the cavity-mediated interactions among two-component bosons are effectively described by long-range spin-spin couplings [38,39]. These couplings are responsible for a class of magnetic phases, some of which have been successfully realized of late [38,40]. Note that the spin-spin interactions involved in this research are purely induced by cavity fields, whereas the intrinsic short-range collisional interaction is absent. An understanding of quantum phases which are born out of the competition between the short- and long-range interactions in a two-component lattice bosons is thus appealing.

In this paper, we consider a two-component ultracold Bose gas subject to cavity-assisted Raman coupling in a two-dimensional optical lattice. Adiabatically eliminating the cavity field, the system can be effectively described by an extended Bose-Hubbard model with both the on-site and dynamic long-range interactions. Using a self-consistent mean-field approach, we obtain the ground-state phase diagrams and analyze the type of the involved transitions. It is shown that the system displays the superfluid, lattice supersolid [41], Mott insulator,, and spin-density wave phases. In contrast to the single-component case [42–49], this lattice supersolid predicted here is characterized by the coexistence of the superfluid and the spin-density wave. Moreover, for the relatively small long-range interaction, the phase diagrams exhibit a correspondence between the parity of the lattice filling number and the spin imbalance. Finally, we propose how to detect the different quantum phases under current experimental setups.

*chengang971@163.com

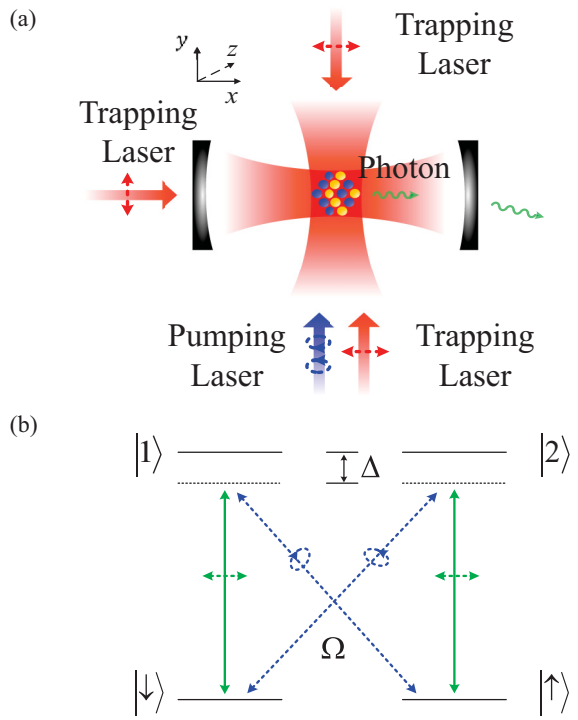

FIG. 1. (a) Schematic of the proposed experimental setup. Two-component bosons confined in a two-dimensional optical lattice are loaded in a cavity, which is subject to a pumping laser. (b) The atomic energy levels and their transitions. Here we take ^{87}Rb atom as an example. Two ground states are chosen as two Zeeman sublevels of $5^2S_{1/2}$, $|F=2, m_F=-2\rangle = |\uparrow\rangle$ and $|F=1, m_F-1\rangle = |\downarrow\rangle$, where F is the total angular momentum and m_F is the magnetic quantum number. While two excited states are chosen as $|F=2, m_F=-1\rangle = |1\rangle$ and $|F=2, m_F=-2\rangle = |2\rangle$ of $5^2P_{3/2}$. For these four energy levels, the pumping laser and the cavity field for governing two separate Raman processes should be circularly and linearly polarized, respectively. The definition of different labels can be seen in the main text.

II. MODEL AND HAMILTONIAN

We consider a two-component ultracold gas of bosonic atoms confined tightly in a two-dimensional (xy) square optical lattice with the strength V_0, as shown in Fig. 1(a). The atoms experience the fundamental mode of a high-finesse optical cavity along the x direction and a transverse pumping laser along the y direction. The cavity field and the pumping laser define two separate Raman processes (we take the z direction as the quantization axis), coupling two hyperfine ground states ($|\uparrow\rangle, |\downarrow\rangle$) of the atoms [see Fig. 1(b) and its caption for details]. The frequency of the pumping laser ω_p is close to that of the cavity mode ω_c, both of which are red detuned from two excited states ($|1\rangle, |2\rangle$) by a large two-photon detuning $|\Delta| \gg \{|g_0|, |\Omega_0|\}$, where g_0 and Ω_0 are the Rabi frequencies of the cavity field and the pumping laser, respectively. The scattered light of the pumping laser oscillates resonantly along the longitude direction of the cavity, mediating an effective long-range atom-atom interaction.

For the deep background optical lattice, the effective Hamiltonian for describing such a system is written in the tight-binding approximation as (see Appendix for details)

$$\hat{H} = -\mu \sum_{j,\sigma} \hat{n}_{j,\sigma} - t \sum_{\langle i,j\rangle,\sigma} (\hat{d}^\dagger_{i,\sigma}\hat{d}_{j,\sigma} + \text{H.c.}) + V \sum_{j,\sigma} \hat{n}_{j,\sigma}(\hat{n}_{j,\sigma}-1) + V_{\uparrow\downarrow} \sum_j \hat{n}_{j,\uparrow}\hat{n}_{j,\downarrow} - \frac{U}{L}\left(\sum_e \hat{d}^\dagger_{e,\uparrow}\hat{d}_{e,\downarrow} - \sum_o \hat{d}^\dagger_{o,\uparrow}\hat{d}_{o,\downarrow} + \text{H.c.}\right)^2. \quad (1)$$

In the Hamiltonian (1), the operator $\hat{d}^\dagger_{j,\sigma}$ ($\hat{d}_{j,\sigma}$) creates (annihilates) a boson with spin σ at lattice site j and $\hat{n}_{j,\sigma} = \hat{d}^\dagger_{j,\sigma}\hat{d}_{j,\sigma}$. The symbol $\langle i, j\rangle$ indicates that the summation runs over all pairs of nearest-neighboring sites and the subscript $e(o)$ means that the lattice sites $i = (i_x, i_y)$ obey $i_x + i_y \in$ even (odd). μ is the chemical potential, t is the hopping rate of the nearest-neighboring site, V ($V_{\uparrow\downarrow}$) is the on-site intraspin (interspin) interaction strength, and H.c. is the Hermitian conjugate. The last term of the right part of the Hamiltonian (1) models the cavity-mediated long-range interaction with the strength

$$U = -\frac{L|\eta M_0|^2\tilde{\delta}}{\tilde{\delta}^2+\kappa^2}, \quad (2)$$

where L is the lattice size, κ is the cavity decay rate, $\eta = g_0\Omega_0/(2\Delta)$ is the two-photon Rabi frequency, $\tilde{\delta} = \Delta_c - NM_1$ is the effective cavity detuning with N being the total atom number and $\Delta_c = \omega_p - \omega_c$, $M_0 = \iint dxdyW_j^*(x,y)\cos(k_0x)\cos(k_0y)W_j(x,y)$ and $M_1 = (g_0^2/\Delta)\iint dxdyW_j^*(x,y)\cos^2(k_0x)W_j(x,y)$ with $W_j(x,y)$ being the Wannier function centered at site j and k_0 being the wave vector of the cavity field. Similarly to the experiment in Ref. [9], this wave vector is here considered to be the same as that of the two-dimensional background lattice potential. Note that the long-range interaction strength U, the short-range interaction strength V ($V_{\uparrow\downarrow}$), and the hopping rate t can be tuned independently by varying the lattice depth V_0, the Rabi frequency Ω_0, and the cavity detuning Δ_c. We assume $U > 0$ hereafter, which can be easily satisfied by letting $\tilde{\delta} < 0$.

Notice that the long-range interaction is proportional to the spin imbalance between the even and odd sites; it is thus expected that a spin-density wave structure may come out of the present atom-photon coupling.

III. GROUND-STATE PROPERTIES

In order to access the ground-state properties of our considered two-dimensional system, the mean-field decoupling approximation is usually used to simplify the Hamiltonian (1) [9,31,42,43,50–53]. Since the infinite-range interaction $\hat{\Theta}^2 = [\sum_e(\hat{d}^\dagger_{e,\uparrow}\hat{d}_{e,\downarrow} + \hat{d}^\dagger_{e,\downarrow}\hat{d}_{e,\uparrow}) - \sum_o(\hat{d}^\dagger_{o,\uparrow}\hat{d}_{o,\downarrow} + \hat{d}^\dagger_{o,\downarrow}\hat{d}_{o,\uparrow})]^2$, it usually makes the system favor the different spins between the even and odd sites when lowering the energy of the Hamiltonian (1), which indicates the possible occurrence of the broken of the Z_2 symmetry of spin. When considering this fact, we decouple this infinite-range interaction by introducing the order parameter $\theta = \langle(\hat{d}^\dagger_{e,\uparrow}\hat{d}_{e,\downarrow} + \hat{d}^\dagger_{e,\downarrow}\hat{d}_{e,\uparrow}) - (\hat{d}^\dagger_{o,\uparrow}\hat{d}_{o,\downarrow} + \hat{d}^\dagger_{o,\downarrow}\hat{d}_{o,\uparrow})\rangle$, which describes the average spin imbalance between the even and odd sites [42,43,45]. If neglecting the term quadratic in fluctuations, then $\hat{\Theta}^2 \approx 2\langle\hat{\Theta}\rangle\hat{\Theta} - \langle\hat{\Theta}\rangle^2 = L\theta\hat{\Theta} - L^2\theta^2/4$. On the other hand, the hopping term is generally

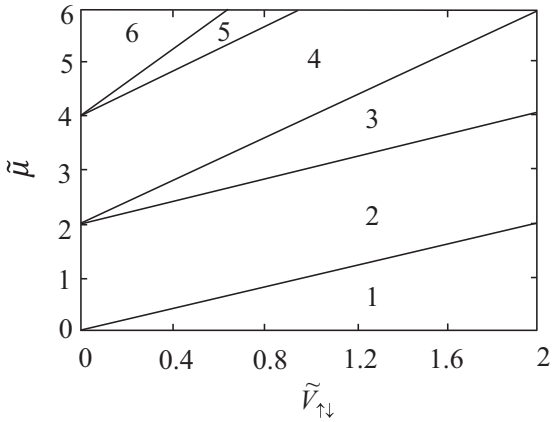

FIG. 2. Phase diagram in the $\tilde{V}_{\uparrow\downarrow}$-$\tilde{\mu}$ plane with $\tilde{t}=0$ and $\tilde{U}=0$. The quantum phases differ from each other by their filling numbers n denoted in the diagram.

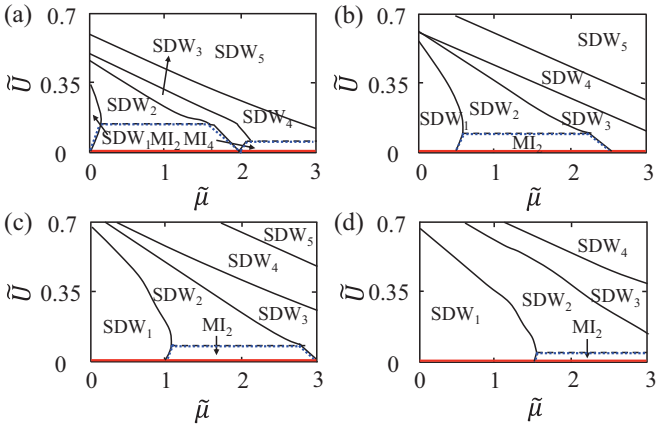

FIG. 3. Phase diagrams in the $\tilde{\mu}$-$\tilde{U}$ plane with $\tilde{t}=0$ for (a) $\tilde{V}_{\uparrow\downarrow}=0$, (b) $\tilde{V}_{\uparrow\downarrow}=0.5$, (c) $\tilde{V}_{\uparrow\downarrow}=1$, and (d) $\tilde{V}_{\uparrow\downarrow}=1.5$. MI$_n$ and SDW$_n$ denote the Mott insulator and spin-density wave phases, which are specified by the filling number n. The solid and dashed lines denote the first- and second-order transitions, respectively. The blue dots indicate the analytical results according to Eqs. (9), (11), and (12). The red solid line at $\tilde{U}=0$ denotes the Mott insulator.

decoupled through the site-independent superfluid order parameter [50]. However, in our case the superfluid order parameters between the even and odd sites might be different due to the possible occurrence of the broken of the Z_2 symmetry. This means that we should introduce four superfluid order parameters $\phi_{e/o,\sigma}=\langle\hat{d}_{e/o,\sigma}\rangle$ [31,43,44], from which $\hat{d}^\dagger_{e,\sigma}\hat{d}_{o,\sigma}+\hat{d}^\dagger_{o,\sigma}\hat{d}_{e,\sigma}\approx\phi_{e,\sigma}(\hat{d}_{o,\sigma}+\hat{d}^\dagger_{o,\sigma})+\phi_{o,\sigma}(\hat{d}_{e,\sigma}+\hat{d}^\dagger_{e,\sigma})-2\phi_{e,\sigma}\phi_{o,\sigma}$.

Based on the above mean-field decoupling approximation, the Hamiltonian (1) reduces to an effective two-site Hamiltonian

$$\begin{aligned}\frac{2\hat{H}_M}{L}=&-\mu\sum_\sigma(\hat{n}_{e,\sigma}+\hat{n}_{o,\sigma})-t\sum_\sigma[\phi_{e,\sigma}(\hat{d}_{o,\sigma}+\hat{d}^\dagger_{o,\sigma})\\&+\phi_{o,\sigma}(\hat{d}_{e,\sigma}+d^\dagger_{e,\sigma})-2\phi_{e,\sigma}\phi_{o,\sigma}]\\&+V_{\uparrow\downarrow}(\hat{n}_{e,\uparrow}\hat{n}_{e,\downarrow}+\hat{n}_{o,\uparrow}\hat{n}_{o,\downarrow})\\&+V\sum_\sigma[\hat{n}_{e,\sigma}(\hat{n}_{e,\sigma}-1)+\hat{n}_{o,\sigma}(\hat{n}_{o,\sigma}-1)]\\&-U\theta[(\hat{d}^\dagger_{e,\uparrow}\hat{d}_{e,\downarrow}+\hat{d}^\dagger_{e,\downarrow}\hat{d}_{e,\uparrow})-(\hat{d}^\dagger_{o,\uparrow}\hat{d}_{o,\downarrow}+\hat{d}^\dagger_{o,\downarrow}\hat{d}_{o,\uparrow})]\\&+\frac{U}{2}\theta^2.\end{aligned}\tag{3}$$

The order parameters θ and $\phi_{e/o,\sigma}$ can be determined self-consistently by diagonalizing the mean-field Hamiltonian (3) using an iterative algorithm [54]. The ground state is the superfluid (spin-density wave) if $\phi_{e/o,\sigma}$ (θ) is nonzero, while a lattice supersolid is characterized by the coexistence of the superfluid and the spin-density wave, meaning both $\phi_{e/o,\sigma}$ and θ are nonzero. For simplicity, in the following discussion the system parameters are normalized with respect to the intraspin interaction strength V, i.e., $\tilde{V}_{\uparrow\downarrow}=V_{\uparrow\downarrow}/V$, $\tilde{\mu}=\mu/V$, $\tilde{U}=U/V$, and $\tilde{t}=t/V$. We also consider regime where $\tilde{V}_{\uparrow\downarrow}<2$, which excludes the spatial demixing of the inner components [25,31].

We first discuss the parameter regime which is deep inside the insulating regime ($\tilde{t}=0$). If we further assume the atom-cavity coupling is switched off (i.e., $\tilde{U}=0$), then the Hamiltonian (1) is reduced to a standard two-component Bose-Hubbard model. Figure 2 shows the phase diagram as a function of $\tilde{V}_{\uparrow\downarrow}$ and $\tilde{\mu}$. This phase diagram is fully characterized by the filling number $n=N/L$ [55]. The interspin interaction $\tilde{V}_{\uparrow\downarrow}$ couples the two components of the atoms, leading to the odd filling phases with $n_\uparrow-n_\downarrow=\pm1$. The range of the corresponding chemical potential is given by $n-1+(n-1)\tilde{V}_{\uparrow\downarrow}/2<\tilde{\mu}<(n-1)+(n+1)\tilde{V}_{\uparrow\downarrow}/2$. Since each site in this case is doubly degenerate, the ground state should be 2^L degenerate. This degeneracy is lifted by turning on the atom-cavity coupling (i.e., $\tilde{U}\neq0$). In Fig. 3, we plot the phase diagrams as functions of $\tilde{U}$ and $\tilde{\mu}$ for different $\tilde{V}_{\uparrow\downarrow}$. For small $\tilde{U}$, the ground-state spin texture exhibits an odd-even filling-dependent behavior. That is, the ground-state is the Mott insulator ($\theta=0$) for the even filling, whereas it is the spin-density wave for the odd filling. Increasing $\tilde{U}$ further beyond a critical value $\tilde{U}_c$ (depending on $\tilde{V}_{\uparrow\downarrow}$), all quantum phases become the spin density waves despite their filling numbers. Apart from these common features, the phase diagrams in Figs. 3(a)–3(d) differ from each other by the location of the critical line $\tilde{U}=\tilde{U}_c$ and the basic structure of the phase boundaries. In Fig. 4, we plot the phase diagrams as functions of $\tilde{V}_{\uparrow\downarrow}$ and $\tilde{U}$. This figure shows that below $\tilde{U}_c$, odd-even filling-dependent behavior also exists. Moreover, with increasing $V_{\uparrow\downarrow}$, $\tilde{U}_c$ decreases linearly.

To get a quantitative understanding of these phase diagrams, we employ a perturbative analysis of the mean-field Hamiltonian (3). In terms of the spin operators $\hat{S}^z_j=(\hat{n}_{j,\uparrow}-\hat{n}_{j,\downarrow})/2$ and $\hat{S}^x_j=(\hat{d}^\dagger_{j,\uparrow}\hat{d}_{j,\downarrow}+\hat{d}^\dagger_{j,\downarrow}\hat{d}_{j,\uparrow})/2$, this Hamiltonian is rewritten as

$$\frac{2\hat{H}}{N}=\hat{H}'+\hat{H}_0,\tag{4}$$

where

$$\begin{aligned}\hat{H}'&=-2\tilde{U}\theta\big(\hat{S}^x_e-\hat{S}^x_o\big),\\\hat{H}_0&=(2-\tilde{V}_{\uparrow\downarrow})\big(\hat{S}^{z2}_e+\hat{S}^{z2}_o\big)+\frac{\tilde{U}}{2}\theta^2\\&\quad+\tfrac{1}{4}(2+\tilde{V}_{\uparrow\downarrow})[(\hat{n}_{e,\uparrow}+\hat{n}_{e,\downarrow})^2+(\hat{n}_{o,\uparrow}+\hat{n}_{o,\downarrow})^2]\\&\quad-(1+\tilde{\mu})(\hat{n}_{e,\uparrow}+\hat{n}_{e,\downarrow}+\hat{n}_{o,\uparrow}+\hat{n}_{o,\downarrow}).\end{aligned}\tag{5}$$

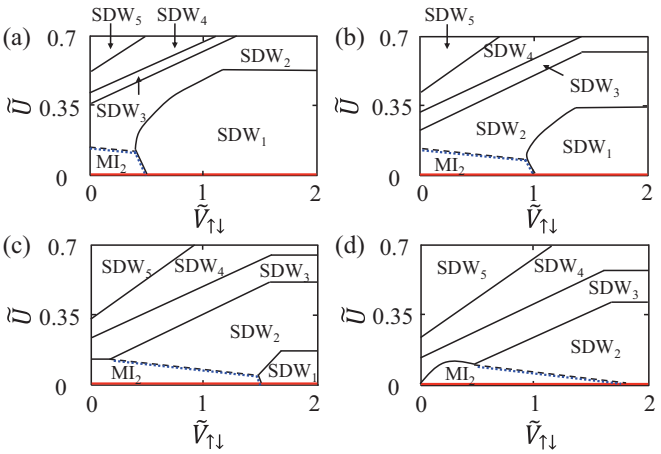

FIG. 4. Phase diagrams in the $\tilde{V}_{\uparrow\downarrow}$-$\tilde{U}$ plane with $\tilde{t} = 0$ for (a) $\tilde{\mu} = 0.5$, (b) $\tilde{\mu} = 1$, (c) $\tilde{\mu} = 1.5$, and (d) $\tilde{\mu} = 2$. The solid and dashed lines denote the first- and second-order transitions, respectively. The blue dots indicate the analytical results according to Eqs. (9), (11), and (12). The red solid line at $\tilde{U} = 0$ denotes the Mott insulator.

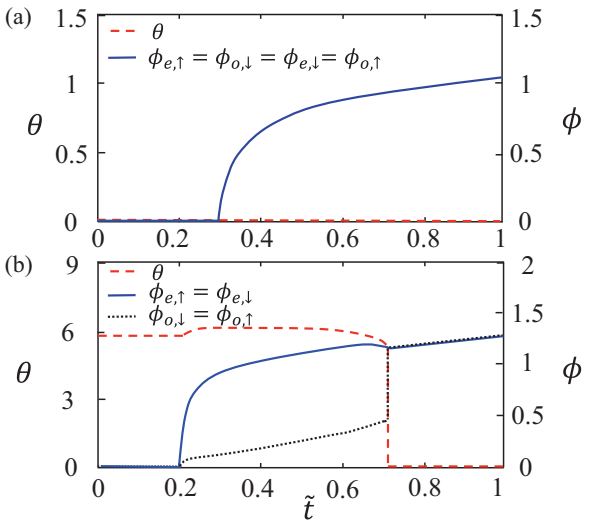

FIG. 5. The order parameters θ and $\phi_{e/o,\sigma}$ as functions of $\tilde{t}$ for (a) $\{\tilde{U} = 0.1, \tilde{V}_{\uparrow\downarrow} = 0.3, \tilde{\mu} = 1.5\}$ and (b) $\{\tilde{U} = 0.4, \tilde{V}_{\uparrow\downarrow} = 0.5, \tilde{\mu} = 1\}$.

For small $\tilde{U}$, $\hat{H}'$ is a perturbation of $\hat{H}_0$. The eigenstate of $\hat{H}_0$ is naturally chosen as the Dicke state, which is the simultaneous eigenstate of the collective spin angular momentum $\hat{S}$ and its z component $\hat{S}^z$. For the filling number n, the Dicke state is expressed as $|n/2, m_{e/o}\rangle$, which obeys $\hat{S}_e^z|n/2, m_e\rangle = m_e|n/2, m_e\rangle$ and $\hat{S}_o^z|n/2, m_o\rangle = m_o|n/2, m_o\rangle$. In terms of this eigenstate, the eigenenergy

$$E_0 = (2 - \tilde{V}_{\uparrow\downarrow})\left(m_e^2 + m_o^2\right) + \frac{\tilde{U}}{2}\theta^2 + \frac{1}{2}(2 + \tilde{V}_{\uparrow\downarrow})n^2 - 2(1 + \tilde{\mu})n. \tag{6}$$

The ground-state energy requires $m_e = m_o = 0$ for the even filling, and $m_e = \pm 1/2$ and $m_o = \pm 1/2$ for the odd filling. This means that for the even filling the ground state is nondegenerate, while it becomes quadruple degenerate for the odd filling. As a result, the total ground-state energies of $\hat{H}$ for the even and odd fillings are quite different.

For the even filling, the second-order perturbative ground-state energy of $\hat{H}$ is calculated as

$$E^0_{\text{even}} = \tfrac{1}{2}(2 + \tilde{V}_{\uparrow\downarrow})n^2 - 2(1 + \tilde{\mu})n + \beta\theta^2, \tag{7}$$

where the coefficient

$$\beta = \frac{\tilde{U}}{2} - \frac{4\tilde{U}^2}{2 - \tilde{V}_{\uparrow\downarrow}}\left[\frac{n}{2}\left(\frac{n}{2} + 1\right)\right]. \tag{8}$$

The choice of θ (zero or a finite value) is determined by the sign change of β [56]. This indicates that the critical value of $\tilde{U}$ can be found with $\beta = 0$, i.e.,

$$\tilde{U}_c = \frac{2 - \tilde{V}_{\uparrow\downarrow}}{2n^2 + 4n}. \tag{9}$$

When $\tilde{U} < \tilde{U}_c$, $\beta > 0$, i.e., $\theta = 0$, which means that the system is in the Mott insulator phase. As $\tilde{U} > \tilde{U}_c$, $\beta < 0$, i.e., θ becomes nonzero which indicates that the system enters into the spin-density wave phase.

For the odd filling, the first-order perturbative ground-state energy of $\hat{H}$ is calculated as $E^{(1)}_{01} = -\tilde{U}\theta(n + 1)$, $E^{(1)}_{02} = \tilde{U}\theta(n + 1)$, $E^{(1)}_{03} = 0$, and $E^{(1)}_{04} = 0$. For lowering the energy, θ should be nonzero, which shows that the system is always in the spin-density wave phase. This, together with the fact of the even filling, explains an odd-even-filling-dependent behavior in Fig. 3.

Since $E^{(1)}_{01}$ and $E^{(1)}_{02}$ are symmetric with respect to $\tilde{U}\theta$, here we choose $\theta > 0$ for simplicity. In this case, the zero-order wave function of $\hat{H}$ is given by $|\Psi^{(0)}\rangle = 1/2(-|n/2, 1/2\rangle|n/2, 1/2\rangle + |n/2, 1/2\rangle|n/2, -1/2\rangle - |n/2, -1/2\rangle|n/2, 1/2\rangle + |n/2, -1/2\rangle|n/2, -1/2\rangle)$, from which $\theta = 2\langle\hat{S}_e^x - \hat{S}_o^x\rangle = 1/2(n + 1)$. Thus, the first-order perturbative ground-state energy is given finally as

$$E^0_{\text{odd}} = \frac{2 - \tilde{V}_{\uparrow\downarrow}}{2} + \frac{2 + \tilde{V}_{\uparrow\downarrow}}{2}n^2 - 2(1 + \tilde{\mu})n - \frac{3\tilde{U}}{8}(n + 1)^2. \tag{10}$$

Since in the case of $\tilde{U} < \tilde{U}_c$ the ground-state energy of the phase boundary for the even filling is equal to that of the odd filling, we have

$$\tilde{U} = \frac{8[2(\mu - n) - n\tilde{V}_{\uparrow\downarrow}]}{3(n + 1)^2}, \tag{11}$$

$$\tilde{U} = \frac{8[2(1 + \mu - n) - \tilde{V}_{\uparrow\downarrow}(1 + n)]}{3(1 + n)^2}. \tag{12}$$

Equations (9), (11), and (12) completely summarize the phase boundaries for $\tilde{U} < \tilde{U}_c$ with $\tilde{t} = 0$. They are in great agreement with the numerical results obtained by the self-consistent mean-field treatment, as shown in Figs. 3 and 4.

Having understood the physics in the insulating limit, we now switch on the atom hopping $\tilde{t}$ and see what happens. Before characterizing the full phase diagram, it is instructive to catch some intuitive insights into the evolution of the order parameters with respect to $\tilde{t}$. As an exemplary case, Figs. 5(a) and 5(b) show the impacts of a finite $\tilde{t}$ on the Mott

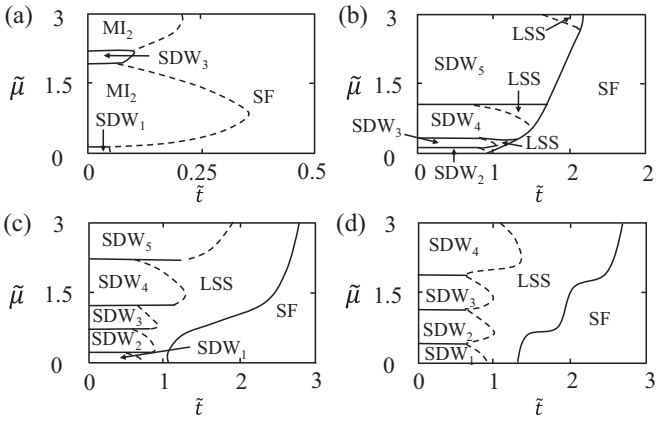

FIG. 6. Phase diagrams in the $\tilde{t}$-$\tilde{\mu}$ plane for (a) $\{\tilde{V}_{\uparrow\downarrow} = 0,\ \tilde{U} = 0.04\}$, (b) $\{\tilde{V}_{\uparrow\downarrow} = 0,\ \tilde{U} = 0.4\}$, (c) $\{\tilde{V}_{\uparrow\downarrow} = 0.5,\ \tilde{U} = 0.4\}$, and (d) $\{\tilde{V}_{\uparrow\downarrow} = 1,\ \tilde{U} = 0.4\}$. The solid and dashed lines denote the first- and second-order transitions, respectively. SF and LSS denotes the superfluid and lattice supersolid phases, respectively.

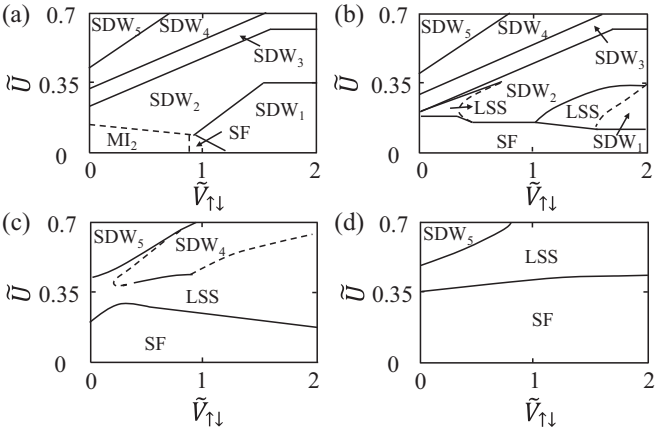

FIG. 7. Phase diagrams in the $\tilde{V}_{\uparrow\downarrow}$-$\tilde{U}$ plane with $\tilde{\mu} = 1$ for (a) $\tilde{t} = 0.1$, (b) $\tilde{t} = 0.5$, (c) $\tilde{t} = 1$, and (d) $\tilde{t} = 2$. The solid and dashed lines denote the first- and second-order transitions, respectively.

insulator and spin-density wave phases, respectively. As shown in Fig. 5(a), an increasing atom hopping directly drives the system from the Mott insulator phase to the superfluid phase with the broken of the $U(1)$ symmetry. Whereas in Fig. 5(b), as $\tilde{t}$ increases, the system goes into the superfluid phase from the Mott insulator phase with an intermediate region ($\phi_{e/o,\sigma} \neq 0,\ \theta \neq 0,\ \phi_{e,\sigma} \neq \phi_{o,\sigma}$) sitting in between. In this region, the Z_2 and U(1) symmetries are broken simultaneously.

In Fig. 6, we plot the phase diagrams as functions of $\tilde{t}$ and $\tilde{\mu}$ for different $\tilde{U}$ and $\tilde{V}_{\uparrow\downarrow}$. The quantum phases for the small hopping strength basically follow those of zero hopping. That is, in the case of $\tilde{U} < \tilde{U}_c$, the Mott insulator and spin-density wave phases alternatively appear as $\tilde{\mu}$ increases [see Fig. 6(a)]. For $\tilde{U} > \tilde{U}_c$, only the spin-density wave phase can be found [see Figs. 6(b)–6(d)]. When $\tilde{U}$ is small, the spin-density wave phase becomes the superfluid phase through a first-order transition with increasing $\tilde{t}$ [see Fig. 6(a)]. For strong $\tilde{U}$, further increasing $\tilde{t}$, the system undergoes a second-order transition from the spin-density wave phase to the lattice supersolid phase and eventually reaches the superfluid phase in the large-$\tilde{t}$ limit through a first-order transition. The lattice supersolid region can be enlarged by increasing either $\tilde{U}$ [see Figs. 6(a)–6(b)] or $\tilde{V}_{\uparrow\downarrow}$ [see Figs. 6(b)–6(d)]. In Fig. 7, we plot the phase diagrams as functions of $\tilde{U}$ and $\tilde{V}_{\uparrow\downarrow}$ for different $\tilde{t}$ with $\tilde{\mu} = 1$. For small $\tilde{t}$, a second-order transition from the Mott insulator phase to the superfluid phase only occurs for a weak $\tilde{U}$ and a strong $\tilde{V}_{\uparrow\downarrow}$ [see Fig. 7(a)]. With increasing $\tilde{t}$, first- and second-order transitions from the superfluid and spin-density wave phases to the lattice supersolid phase emerge, respectively [see Fig. 7(b)]. For strong $\tilde{t}$, the lattice supersolid phase emerges at a strong $\tilde{U}$ [see Figs. 7(c) and 7(d)]. The broken symmetries of the phase transitions in Figs. 6 and 7 are summarized in Table I.

Notice that fixing the particle number is more experimentally realistic than specifying the chemical potential, and, as expected from above discussions, the parity of the particle filling may play an important role in defining the insulating character of the ground state. Therefore, in Fig. 8 we plot the phase diagrams as functions of $\tilde{t}$ and $\tilde{U}$ for two representative fillings, $n = 2$ and $n = 3$. Figure 8(a) shows the phase diagram for the even filling, $n = 2$. It is observed that for small $\tilde{t}$, a second-order transition between the Mott insulator and spin density wave phases takes place at $\tilde{U} = \tilde{U}_c$. On increasing $\tilde{t}$, we find the usual second-order transition from the Mott insulator phase to the superfluid phase in the case of $\tilde{U} < \tilde{U}_c$. While for $\tilde{U} > \tilde{U}_c$, the spin-density wave phase first crosses the lattice supersolid region and then undergoes a first-order transition to the superfluid phase. In Fig. 8(b), we plot the phase diagram for the odd filling, $n = 3$. In this case, no Mott insulator phase exists and one instead observes a first-order transition between the spin-density wave and superfluid phases for small $\tilde{U}$. For increasing $\tilde{U}$, the lattice supersolid phase appears, separating the spin-density wave and superfluid phases. The broken symmetries of the phase transitions in Fig. 8 are also summarized in Table I.

IV. PARAMETER ESTIMATION AND POSSIBLE EXPERIMENTAL OBSERVATION

We estimate the parameters based on recent experiments where ^{87}Rb ultracold atoms load in an optical cavity [9,38]. In these experiments, about $4.2(4) \times 10^4$ atoms are trapped in the two-dimensional background optical lattice with the wavelength $\lambda = 785.3$ nm. The corresponding recoil energy is $E_r = h^2/(2m\lambda^2) \sim 10$ kHz (m is the atomic mass). We

TABLE I. The broken symmetries and orders of the different transitions in the phase diagrams (6), (7), and (8) ($n \neq n'$).

Quantum phase transition	Symmetry broken	Order
MI_n-SF	$U(1)$	Second
SDW_n-LSS	$U(1)$	Second or First
LSS-SF	Z_2	First
MI_n-$\mathrm{SDW}_n(\mathrm{SDW}_{n'})$	Z_2	Second (First)
SDW_n-SF	$U(1), Z_2$	First
SDW_n-$\mathrm{SDW}_{n'}$	Ø	First

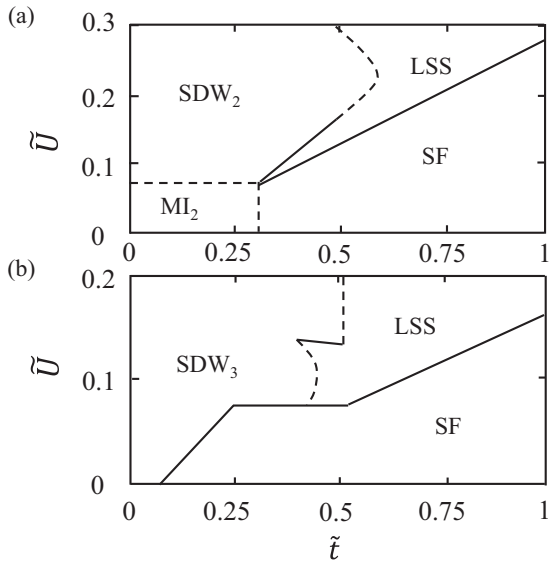

FIG. 8. Phase diagrams in the $\tilde{t}$-$\tilde{U}$ plane with $\tilde{V}_{\uparrow\downarrow} = 0.5$ for (a) $n = 2$ and (b) $n = 3$. The solid and dashed lines denote the first- and second-order transitions, respectively.

choose two Zeeman sublevels of $5^2S_{1/2}$, $|F, m_F\rangle = |1, -1\rangle = |\downarrow\rangle$, and $|F, m_F\rangle = |2, -2\rangle = |\uparrow\rangle$ as an example. This choice has two advantages. One is that the ratio of the interaction strengths $V_{\uparrow\downarrow}$ and V can be tuned experimentally by the inter-spin Feshbach resonance [57]. The other is that these Zeeman sublevels can be well coupled by two Raman processes. In this case, the two-photon detuning $|\Delta|$ can be set about 100 GHz [38] and $(|g_0|, |\Omega_0|, |\Delta_c|)$ can be set to be on the order of a few MHz [9]. Since $|\Delta| \gg \{|g_0|, |\Omega_0|, |\Delta_c|\}$, the adiabatic elimination can be well satisfied. In typical experiments [8,9], the cavity decay rate $\kappa \sim 10$ MHz is much larger than the recoil energy, and the steady-state approximation can thus be applied safely. When the lattice depth V_0 is adjusted from $3E_r$ to $18E_r$ and Δ_c is tuned below $-2\pi \times 18.3$ MHz, the energy scales, including $2V$, $V_{\uparrow\downarrow}$, U and t, are at least five times smaller than the gap between the lowest and first excited Bloch bands [9]. As a result, the single-band approximation in deriving the effective Hamiltonian (1) is valid [9].

Finally, we propose how to detect the different quantum phases. The superfluid and Mott insulator can be distinguished by measuring the BEC fraction $f = N_c/N$ (N_c is the coherent atom number). f is determined by observing the interference pattern with absorption images of atomic cloud in momentum space [1,9]. In the superfluid phase, $f \neq 0$, while in the Mott insulator phase, $f = 0$. Since $\theta \approx \sqrt{n_{\rm ph}(\Delta_c^2/\eta^2)}$ ($n_{\rm ph}$ is the intracavity photon number) [9], the spin-density wave phase can be determined by detecting the intracavity photon number, and the lattice supersolid is characterized by nonzero f and $n_{\rm ph}$.

V. CONCLUSION

In summary, by considering a two-component atomic Bose lattice gas inside an optical cavity, we have explored a novel competition between the short-range collisional and cavity-mediated long-range interactions. We have shown that this competition generates rich ground-state phase diagrams showing the superfluid, lattice supersolid, Mott insulator, and spin-density wave phases. Unlike its single-component analog, this lattice supersolid predicted here is characterized by the coexistence of the superfluid and the spin-density wave. Moreover, for the relatively small long-range interaction, the phase diagrams exhibit a correspondence between the parity of the lattice filling number and the spin imbalance. Finally, we have proposed how to detect the different quantum phases under current experimental setups.

ACKNOWLEDGMENTS

This work is supported partly by the National Key R&D Program of China under Grant No. 2017YFA0304203, the NSFC under Grants No. 11674200 and No. 11804204, and 1331KSC.

APPENDIX: THE DERIVATION OF THE EFFECTIVE HAMILTONIAN (1)

In this Appendix, we present the detailed derivation of the Hamiltonian (1). We start with a single-atom time-dependent Hamiltonian $\hat{H}^{(1)}(t) = \hat{H}_{\rm A}^{(1)} + \hat{H}_{\rm A\text{-}P}^{(1)}(t)$, where

$$\hat{H}_{\rm A}^{(1)} = \sum_{i=1,2,\uparrow,\downarrow} \omega_i |i\rangle\langle i| + \omega_c \hat{a}^\dagger \hat{a} + \frac{\mathbf{p}_{x,y}^2}{2m} + V_0[\cos^2(k_0 x) + \cos^2(k_0 y)], \quad \text{(A1)}$$

$$\hat{H}_{\rm A\text{-}P}^{(1)}(t) = \frac{\Omega(y)}{2} e^{-i\omega_p t}(|1\rangle\langle\uparrow| + |2\rangle\langle\downarrow|) + g(x)\hat{a}(|1\rangle\langle\downarrow| + |2\rangle\langle\uparrow|) + \text{H.c.} \quad \text{(A2)}$$

In the Hamiltonian $H_{\rm A}^{(1)}$, ω_i is the eigenfrequency of the internal state $|i\rangle$. For simplicity, we take $\omega_1 = \omega_2 = \omega_A$ and $\omega_\uparrow = \omega_\downarrow = 0$. $p_{x,y}$ and m are the momentum and mass of the atoms, respectively. V_0 and k_0 are the depth and the wave vector of the two-dimensional background lattice potential, respectively. This wave vector is the same as that of the cavity field. In the Hamiltonian $\hat{H}_{\rm A\text{-}P}^{(1)}(t)$, $\Omega(y) = \Omega_0 \cos(k_0 y)$ and $g(x) = g_0 \cos(k_0 x)$ are the spatial-dependent Rabi frequency and atom-cavity coupling strength, respectively.

By performing a unitary transformation operator, $\hat{U}(t) = \exp[i\omega_p t(\hat{a}^\dagger\hat{a} + |1\rangle\langle 1| + |2\rangle\langle 2|)]$, the time-dependent Hamiltonian $H^{(1)}(t)$ becomes

$$\hat{H}^{(2)} = -\Delta_c \hat{a}^\dagger\hat{a} + \frac{\mathbf{p}_{x,y}^2}{2m} + V_0[\cos^2(k_0 x) + \cos^2(k_0 y)] - \Delta(|1\rangle\langle 1| + |2\rangle\langle 2|) + \frac{1}{2}[\Omega(y)(|1\rangle\langle\uparrow| + |2\rangle\langle\downarrow|) + g(x)\hat{a}(|1\rangle\langle\downarrow| + |2\rangle\langle\uparrow|)] + \text{H.c.}, \quad \text{(A3)}$$

where $\Delta_c = \omega_p - \omega_c$ and $\Delta = \omega_p - \omega_A$. As $|\Delta| \gg \{|g_0|, |\Omega_0|, |\Delta_c|\}$, the excited states $|1\rangle$ and $|2\rangle$ can be eliminated adiabatically. The effective Hamiltonian reduces to

$$H^{(3)} = (\omega - \Delta_c)\hat{a}^\dagger\hat{a} + \frac{\mathbf{p}_{x,y}^2}{2m} + V_0[\cos^2(k_0 x) + \cos^2(k_0 y)] + \eta\cos(k_0 x)\cos(k_0 y)(|\downarrow\rangle\langle\uparrow| + |\uparrow\rangle\langle\downarrow|)(\hat{a}^\dagger + \hat{a}), \quad \text{(A4)}$$

where $\eta = g_0\Omega_0/(2\Delta)$ and $\omega = |g_0|^2\cos^2(k_0 x)/\Delta$.

We now incorporate the short-range contact interactions between the atoms. The extended many-body Hamiltonian can be written as

$$\hat{H}^{(4)} = \sum_{\sigma} \iint dxdy \hat{\psi}_{\sigma}^{\dagger}(x,y) \left[\frac{\mathbf{p}_{x,y}^2}{2m} + V_0(x,y) - \mu + \omega \hat{a}^{\dagger}\hat{a} \right] \hat{\psi}_{\sigma}(x,y) + V_{\uparrow\uparrow}^{2d} \iint dxdy \hat{\psi}_{\uparrow}^{\dagger}(x,y)\hat{\psi}_{\uparrow}^{\dagger}(x,y)\hat{\psi}_{\uparrow}(x,y)\hat{\psi}_{\uparrow}(x,y)$$
$$+ V_{\downarrow\downarrow}^{2d} \iint dxdy \hat{\psi}_{\downarrow}^{\dagger}(x,y)\hat{\psi}_{\downarrow}^{\dagger}(x,y)\hat{\psi}_{\downarrow}(x,y)\hat{\psi}_{\downarrow}(x,y) + V_{\uparrow\downarrow}^{2d} \iint dxdy \hat{\psi}_{\uparrow}^{\dagger}(x,y)\hat{\psi}_{\downarrow}^{\dagger}(x,y)\hat{\psi}_{\downarrow}(x,y)\hat{\psi}_{\uparrow}(x,y)$$
$$+ \eta(\hat{a}^{\dagger} + \hat{a}) \iint dxdy [\hat{\psi}_{\uparrow}^{\dagger}(x,y)\hat{\psi}_{\downarrow}(x,y) + \hat{\psi}_{\downarrow}^{\dagger}(x,y)\hat{\psi}_{\uparrow}(x,y)] \cos(k_0 x)\cos(k_0 y) - \Delta_c \hat{a}^{\dagger}\hat{a}. \tag{A5}$$

In the Hamiltonian (A5), $\hat{\psi}_{\sigma}(x,y)$ denotes the field operator at position (x,y) with the internal state σ ($\sigma = \uparrow, \downarrow$). $V_{\uparrow\uparrow}^{2d} = V_{\downarrow\downarrow}^{2d} = 2\pi a_{s\uparrow\uparrow/\downarrow\downarrow}\hbar^2/(m\pi\rho^2) = V^{2d}$ and $V_{\uparrow\downarrow}^{2d} = 4\pi a_{s\uparrow\downarrow}\hbar^2/(m\pi\rho^2)$ are the contact interaction strengths between the atoms with the same and different internal states, respectively. $a_{s\uparrow\uparrow/\downarrow\downarrow}$ and $a_{s\uparrow\downarrow}$ are the two-body scattering lengths of the same and different internal states, respectively. ρ is a radial characteristic length.

Since here we consider the deep background optical lattice, the field operator $\hat{\psi}_{\sigma}(x,y)$ can be expanded by the lowest-band Wannier function $W_i(x,y) = W(x - x_i, y - y_i)$, i.e., $\hat{\psi}_{\sigma}(x,y) = \sum_{i,\sigma} \hat{d}_{i,\sigma} W_i(x,y)$, where $\hat{d}_{i,\sigma}$ is the operator annihilating a single particle with internal state σ at site i. Therefore the single-band tight-binding Hamiltonian is

$$\hat{H}^{(5)} = (-\Delta_c + M_1 N)\hat{a}^{\dagger}\hat{a} - t\sum_{i,\sigma}(\hat{d}_{i,\sigma}^{\dagger}\hat{d}_{i+1,\sigma} + \text{H.c.}) + \eta(\hat{a}^{\dagger} + \hat{a})M_0 \sum_{i_x,i_y}(-1)^{i_x+i_y}(\hat{d}_{i,\uparrow}^{\dagger}\hat{d}_{i,\downarrow} + \hat{d}_{i,\downarrow}^{\dagger}\hat{d}_{i,\uparrow})$$
$$+ V\sum_{j,\sigma}\hat{n}_{j,\sigma}(\hat{n}_{j,\sigma} - 1) + V_{\uparrow\downarrow}\sum_{j}\hat{n}_{j,\uparrow}\hat{n}_{j,\downarrow} - \mu\sum_{j,\sigma}\hat{n}_{j,\sigma}, \tag{A6}$$

where

$$\hat{n}_{j,\sigma} = \hat{d}_{j,\sigma}^{\dagger}\hat{d}_{j,\sigma}$$
$$t = \iint dxdy W_i^*(x,y)\left[\frac{\mathbf{p}_{x,y}^2}{2m} + V_0(x,y)\right]W_{i+1}(x,y), \quad M_0 = \iint dxdy W_i^*(x,y)\cos(k_0 x)\cos(k_0 y)W_i(x,y),$$
$$M_1 = \frac{|g_0|^2}{\Delta}\iint dxdy W_i^*(x,y)\cos^2(k_0 x)W_i(x,y), \quad V = V^{2d}\iint dxdy|W_i^*(x,y)|^4,$$
$$V_{\uparrow\downarrow} = V_{\uparrow\downarrow}^{2d}\iint dxdy|W_i^*(x,y)|^4.$$

For situations where the cavity-photon decays much faster than the atomic degree of freedom, we are allowed to adiabatically eliminate the cavity field by equating the annihilation operator $\hat{a}$ with its steady-state value, i.e.,

$$\hat{a} = \frac{\eta M_0}{i\kappa + \tilde{\delta}}\sum_{i_x,i_y}(-1)^{i_x+i_y}(\hat{d}_{i,\uparrow}^{\dagger}\hat{d}_{i,\downarrow} + \hat{d}_{i,\downarrow}^{\dagger}\hat{d}_{i,\uparrow}), \tag{A7}$$

where $\tilde{\delta} = \Delta_c - M_1 N$. Substituting Eq. (A7) into the Hamiltonian (A6) yields the Hamiltonian (1) in the main text.

[1] D. Jaksch, C. Brder, J. I. Cirac, C. W. Gardiner, and P. Zoller, Cold Bosonic Atoms in Optical Lattices, Phys. Rev. Lett. **81**, 3108 (1998).

[2] M. Greiner, O. Mandel, T. Esslinger, T. W. Hänsch, and I. Bloch, Quantum phase transition from a superfluid to a Mott insulator in a gas of ultracold atoms, Nature (London) **415**, 39 (2002).

[3] T. Stöferle, H. Moritz, C. Schori, M. Kohl, and T. Esslinger, Transition From a Strongly Interacting 1D Superfluid to a Mott Insulator, Phys. Rev. Lett. **92**, 130403 (2004).

[4] I. Bloch, J. Dalibard, and W. Zwerger, Many-body physics with ultracold gases, Rev. Mod. Phys. **80**, 885 (2008).

[5] L. Fallani, L. D. Sarlo, J. E. Lye, M. Modugno, R. Saers, C. Fort, and M. Inguscio, Observation of Dynamical Instability for a Bose-Einstein Condensate in a Moving 1D Optical Lattice, Phys. Rev. Lett. **93**, 140406 (2004).

[6] J. Mun, P. Medley, G. K. Campbell, L. G. Marcassa, D. E. Pritchard, and W. Ketterle, Phase Diagram for a Bose-Einstein Condensate Moving in an Optical Lattice, Phys. Rev. Lett. **99**, 150604 (2007).

[7] A. J. Ferris and M. J. Davis, Dynamical instabilities of Bose-Einstein condensates at the band edge in one-dimensional optical lattices, Phys. Rev. A **77**, 012712 (2008).

[8] K. Baumann, C. Guerlin, F. Brennecke, and T. Esslinger, Dicke quantum phase transition with a superfluid gas in an optical cavity, Nature (London) **464**, 1301 (2010).

[9] R. Landig, L. Hruby, N. Dogra, M. Landini, R. Mottl, T. Donner, and T. Esslinger, Quantum phases from competing

short- and long-range interactions in an optical lattice, Nature (London) **532**, 476 (2016).
[10] M. R. Bakhtiari, A. Hemmerich, H. Ritsch, and M. Thorwart, Nonequilibrium Phase Transition of Interacting Bosons in an Intra-Cavity Optical Lattice, Phys. Rev. Lett. **114**, 123601 (2015).
[11] J. Klinder, H. Keßler, M. R. Bakhtiari, M. Thorwart, and A. Hemmerich, Observation of a Superradiant Mott Insulator in the Dicke-Hubbard Model, Phys. Rev. Lett. **115**, 230403 (2015).
[12] C. Georges, J. G. Cosme, L. Mathey, and A. Hemmerich, Light-Induced Coherence in an Atom-Cavity System, Phys. Rev. Lett. **121**, 220405 (2018).
[13] T. Mishra, R. V. Pai, and B. P. Das, Phase separation in a two-species Bose mixture, Phys. Rev. A **76**, 013604 (2007).
[14] S. G. Söyler, B. C. Sansone, N. V. Prokof'ev, and B. V. Svstunov, Sign-alternating interaction mediated by strongly correlated lattice bosons, New J. Phys. **11**, 073036 (2009).
[15] A. Kuklov, N. Prokof'ev, and B. Svistunov, Commensurate Two-Component Bosons in an Optical Lattice: Ground State Phase Diagram, Phys. Rev. Lett. **92**, 050402 (2004).
[16] T. Mishra, B. K. Sahoo, and R. V. Pai, Phase-separated charge-density-wave phase in the two-species extended Bose-Hubbard model, Phys. Rev. A **78**, 013632 (2008).
[17] M. Iskin, Mean-field theory for the Mott-insulator–paired-superfluid phase transition in the two-species Bose-Hubbard model, Phys. Rev. A **82**, 055601 (2010).
[18] P. Chen and M.-F. Yang, Quantum phase transitions in a two-species hard-core boson Hubbard model in two dimensions, Phys. Rev. B **82**, 180510(R) (2010).
[19] M. J. Bhaseen, S. Ejima, M. Hohenadler, A. O. Silver, F. H. L. Essler, H. Fehske, and B. D. Simions, Magnetic properties of the second Mott lobe in pairing Hamiltonians, Phys. Rev. A **84**, 023635 (2011).
[20] T. Ohgoe and N. Kawashima, Quantum Monte Carlo method for pairing phenomena: Supercounterfluid of two-species Bose gases in optical lattices, Phys. Rev. A **83**, 023622 (2011).
[21] S. Mandal, K. Saha, and K. Sengupta, Superfluid-insulator transition of two-species bosons with spin-orbit coupling, Phys. Rev. B **86**, 155101 (2012).
[22] Y. Li, L. He, and W. Hofstetter, Anisotropic pair superfluidity of trapped two-component Bose gases in an optical lattice, New J. Phys. **15**, 093028 (2013).
[23] D. Yamamoto, T. Ozaki, C. A. R. Sá de Melo, and I. Danshita, First-order phase transition and anomalous hysteresis of Bose gases in optical lattices, Phys. Rev. A **88**, 033624 (2013).
[24] A. Hubener, M. Snoek, and W. Hofstetter, Magnetic phases of two-component ultracold bosons in an optical lattice, Phys. Rev. B **80**, 245109 (2009).
[25] F. Lingua, M. Guglielmino, and V. Penna, Demixing effects in mixtures of two bosonic species, Phys. Rev. A **92**, 053610 (2015).
[26] S. Anufriiev and T. A. Zaleski, Multicriticality and interaction-induced first-order phase transitions in mixtures of ultracold bosons in an optical lattice, Phys. Rev. A **94**, 043613 (2016).
[27] G. Ceccarelli, J. Nespolo, A. Pelissetto, and E. Vicari, Bose-Einstein condensation and critical behavior of two-component bosonic gases, Phys. Rev. A **92**, 043613 (2015).
[28] C. Menotti and S. Stringari, Detection of pair-superfluidity for bosonic mixtures in optical lattices, Phys. Rev. A **81**, 045604 (2010).
[29] C. M. Chung, S. Fang, and P. Chen, Quantum and thermal transitions out of the pair-supersolid phase of two-species bosons on a square lattice, Phys. Rev. B **85**, 214513 (2012).
[30] M. Iskin, Strong-coupling expansion for the two-species Bose-Hubbard model, Phys. Rev. A **82**, 033630 (2010).
[31] R. M. Wilson, W. E. Shirley, and S. S. Natu, Anomalous supersolidity in a weakly interacting dipolar Bose mixture on a square lattice, Phys. Rev. A **93**, 011605(R) (2016).
[32] K. Günter, T. Stoferle, H. Moritz, and T. Esslinger, Bose-Fermi Mixtures in a Three-Dimensional Optical Lattice, Phys. Rev. Lett. **96**, 180402 (2006).
[33] S. Ospelkaus, C. Ospelkaus, O. Wille, M. Succo, P. Emst, K. Sengstock, and K. Bongs, Localization of Bosonic Atoms by Fermionic Impurities in a Three-Dimensional Optical Lattice, Phys. Rev. Lett. **96**, 180403 (2006).
[34] E. Wille, F. M. Spiegelhalder, G. Kerner, D. Naik, A. Trenkwalder, G. Hendl, F. Schreck, R. Grimm, T. G. Tiecke, J. T. M. Walraven, S. J. J. M. F. Kokkelmans, E. Tiesinga, and P. S. Julienne, Exploring an Ultracold Fermi-Fermi Mixture: Interspecies Feshbach Resonances and Scattering Properties of ^{6}Li and ^{40}K, Phys. Rev. Lett. **100**, 053201 (2008).
[35] J. Catani, L. De Sarlo, G. Barontini, F. Minardi, and M. Inguscio, Degenerate Bose-Bose mixture in a three-dimensional optical lattice, Phys. Rev. A **77**, 011603(R) (2008).
[36] G. Thalhammer, G. Barontini, L. D. Sarlo, J. Catani, F. Minardi, and M. Inguscio, Double Species Bose-Einstein Condensate with Tunable Interspecies Interactions, Phys. Rev. Lett. **100**, 210402 (2008).
[37] S. Tojo, Y. Taguchi, Y. Masuyama, T. Hayashi, H. Saito, and T. Hirano, Controlling phase separation of binary Bose-Einstein condensates via mixed-spin-channel Feshbach resonance, Phys. Rev. A **82**, 033609 (2010).
[38] R. M. Kroeze, Y. Guo, V. D. Vaidya, J. Keeling, and B. L. Lev, Spinor Self-Ordering of a Quantum Gas in a Cavity, Phys. Rev. Lett. **121**, 163601 (2018).
[39] F. Mivehvar, H. Ritsch, and F. Piazza, A Cavity-QED Toolbox for Quantum Magnetism, Phys. Rev. Lett. **122**, 113603 (2019).
[40] M. Landini, N. Dogra, K. Kroeger, L. Hruby, T. Donner, and T. Esslinger, Formation of a Spin Texture in a Quantum Gas Coupled to a Cavity, Phys. Rev. Lett. **120**, 223602 (2018).
[41] J. Léonard, A. Morales, P. Zupancic, T. Esslinger, and T. Donner, Supersolid formation in a quantum gas breaking a continuous translational symmetry, Nature (London) **543**, 87 (2017).
[42] Y. Chen, Z. Yu, and H. Zhai, Quantum phase transitions of the Bose-Hubbard model inside a cavity, Phys. Rev. A **93**, 041601(R) (2016).
[43] N. Dogra, F. Brennecke, S. D. Huber, and T. Donner, Phase transitions in a Bose-Hubbard model with cavity-mediated global-range interactions, Phys. Rev. A **94**, 023632 (2016).
[44] B. Sundar and E. J. Mueller, Lattice bosons with infinite-range checkerboard interactions, Phys. Rev. A **94**, 033631 (2016).
[45] A. E. Niederle, G. Morigi, and H. Rieger, Ultracold bosons with cavity-mediated long-range interactions: A local mean-field analysis of the phase diagram, Phys. Rev. A **94**, 033607 (2016).
[46] T. Flottat, L. F. Parny, F. Hébert, V. G. Rousseau, and G. G. Batrouni, Phase diagram of bosons in a two-dimensional optical lattice with infinite-range cavity-mediated interactions, Phys. Rev. B **95**, 144501 (2017).

[47] R. Liao, H. J. Chen, D. C. Zheng, and Z. G. Huang, Theoretical exploration of competing phases of lattice Bose gases in a cavity, Phys. Rev. A **97**, 013624 (2018).

[48] B. Blaß, H. Rieger, G. Roósz, and F. Iglói, Quantum Relaxation and Metastability of Lattice Bosons with Cavity-Induced Long-Range Interactions, Phys. Rev. Lett. **121**, 095301 (2018).

[49] J. Panas, A. Kauch, and K. Byczuk, Spectral properties and phase diagram of correlated lattice bosons in an optical cavity within bosonic dynamical mean-field theory, Phys. Rev. B **95**, 115105 (2017).

[50] K. Sheshadri, H. R. Krishnamurthy, R. Pandit, and T. V. Ramakrishnan, Superfluid and insulating phases in an interacting-boson model: Mean-field theory and the RPA, Europhys. Lett. **22**, 257 (1993).

[51] F. Mivehvar, H. Ritsch, and F. Piazza, Superradiant Topological Peierls Insulator Inside an Optical Cavity, Phys. Rev. Lett. **118**, 073602 (2017).

[52] F. Mivehvar, F. Piazza, and H. Ritsch, Disorder-Driven Density and Spin Self-Ordering of a Bose-Einstein Condensate in a Cavity, Phys. Rev. Lett. **119**, 063602 (2017).

[53] F. Mivehvar, S. Ostermann, F. Piazza, and H. Ritsch, Driven-Dissipative Supersolid in a Ring Cavity, Phys. Rev. Lett. **120**, 123601 (2018).

[54] A. Dhar, M. Singh, R. V. Pai, and B. P. Das, Mean-field analysis of quantum phase transitions in a periodic optical superlattice, Phys. Rev. A **84**, 033631 (2011).

[55] M. C. Cha, K. Sengupta, and S. M. Girvin, Superfluid-insulator transitions of two-species bosons in an optical lattice, Phys. Rev. B **72**, 184507 (2005).

[56] Y. Chen, Z. Yu, and H. Zhai, Superradiance of Degenerate Fermi Gases in a Cavity, Phys. Rev. Lett. **112**, 143004 (2014).

[57] A. Widera, O. Mandel, M. Greiner, and S. Kreim, Entanglement Interferometry for Precision Measurement of Atomic Scattering Properties, Phys. Rev. Lett. **92**, 160406 (2004).